InGeO:F Channel Engineering by Fluorination Based on a GeO_2 Buffer Layer with Enhanced Mobility and Negative-Bias Stability

Shundong Hu[1,2,3†], Jiayi Wang[1,2,3†*], Kuo Zhang[1,2,3], Nannan You[1,2,3], Yang Xu[1,2,3], Ling Li[1,3], Shengkai Wang[1,2,3*]
[1]State Key Laboratory of Fabrication Technologies for Integrated Circuits, Institute of Microelectronics, Chinese Academy of Sciences, Beijing 100029, China;
[2]High-Frequency High-Voltage Device and Integrated Circuits R&D Center, Institute of Microelectronics, Chinese Academy of Sciences, Beijing 100029, China;
[3]University of Chinese Academy of Sciences, Beijing 10049, China. †Equal contribution.
Email: wangjiayi2021@ime.ac.cn; wangshengkai@ime.ac.cn.

1. Introduction

Indium oxide (In_2O_3)-based thin-film transistors (TFTs) have been widely used in flat panel display (FPD) and dynamic random-access memory (DRAM) owing to the high carrier mobility, low deposition temperature, and wide bandgap. Although shallow donor-like oxygen vacancies (V_O) can provide electrons as carriers resulting in the high mobility nature of In_2O_3, the instability of V_O compromises its reliability [1]. Previous studies mainly focused on cation doping to stabilize V_O, studies on anion doping remain relatively limited. Here, we choose F as anion dopant due to its highest electronegativity to strength the overall metal to anion (*M-X*) bond. Besides, F/O substitution may release electrons to improve mobility, while F/V_O passivation is expected to enhance device stability. However, fluorination typically damages the surface of the oxide channel, resulting in the degradation of device performance. Based on our previous study, GeO_2 can effectively consume V_O in In_2O_3 [3]. Therefore, GeO_2 can be utilized as a buffer layer, which not only reduces the fluorination damage to the In_2O_3 channel but also achieves controllable F incorporation. Electrical and material characterizations were conducted on three types of devices—pristine In_2O_3, GeO_2-passivated In_2O_3 (InGeO), and fluorinated GeO_2-passivated In_2O_3 (InGeO:F) TFTs—to reveal the F incorporation mechanism and its effect on the electrical characteristics of the InGeO:F transistors.

2. Device Fabrication

Fig. 1(a) and **(b)** present the structure and fabrication process of the InGeO: F TFT, where **Fig. 1(c)** shows its cross-sectional TEM image. The thicknesses of In_2O_3 channel and GeO_2 buffer layer are 5 nm and 7 nm, respectively. The GeO_2/In_2O_3 stack was etched by SF_6 (15 sccm) at 15 W for 60 s. The IZO source/drain electrodes were then deposited. The channel W/L are 150/400 μm, defined by shadow masks. Post-deposition annealing (PDA) was carried out in air at 400 °C for 30 min. **Fig. 1(d)** presents the linear energy-dispersive X-ray spectroscopy (EDS) scan, indicating F is successfully incorporated in the GeO_2 buffer layer and the In_2O_3 channel.

3. Results and Discussion

Fig. 2(a) presents the transfer characteristics (I-V) of In_2O_3, InGeO, and InGeO:F TFTs. The threshold voltage (V_{th}) and mobility (μ_{FE}) extracted from the I-V curves are plotted in **Fig. 2(b)**. The negative-bias stress (NBS) reliability tests were conducted for all three devices with applied $V_G = (V_{th} - 4)$ V for 2000 s, which are displayed in **Fig. 3**. Key electrical factors including V_{th}, μ_{FE}, SS, and ΔV_{th} extracted from **Fig.2** and **3** are listed in **Table I**. Compared with the In_2O_3 TFT, introducing a GeO_2 buffer layer (InGeO TFT) causes a positive shift in V_{th} and a slight decrease in μ_{FE}, while significantly reducing the ΔV_{th} under applied NBS. This suggests that the GeO_2 layer effectively consumes V_O in In_2O_3 without introducing excessive ionized impurity scattering. For the fluorinated InGeO:F TFT, the GeO_2 buffer layer effectively mitigating plasma-induced damage to the In_2O_3 channel, which exhibits the most positive V_{th} , the highest μ_{FE}, the lowest SS, and the smallest ΔV_{th} under NBS (**Table I**). During fluorination, F^- substitutes O^{2-} and bonds with In^{3+} resulting in a more rigid In–O,F frame, which not only suppresses the formation of new V_O but also fills pre-existing ones, thereby reducing the background electron concentration and causing a positive shift in V_{th}. Meanwhile, F eliminates V_O-related scattering centers and improves the local lattice environment by forming stable In–F bonds [4], allowing electrons to transport more smoothly and thus significantly enhancing mobility. In addition, the passivation of V_O and associated defect states lowers the trap-state density at the channel/interface, strengthens the gate control over the channel, and thus reduces SS. Under NBS conditions, the channel energy band bends upward, and neutral V_O are easily activated into charged states, releasing electrons and inducing a negative shift in V_{th} [5]. In contrast, the filling and passivation effect of F shifts the defect levels toward the valence band, effectively suppressing defect transformation and electron release, thereby significantly reducing ΔV_{th} and enhancing device reliability.

To elucidate the origin of the performance enhancement after F doping, secondary ion mass spectrometry (SIMS) and X-ray photoelectron spectroscopy (XPS) were performed on the fluorinated GeO_2/ In_2O_3 stack (InGeO:F). The elemental depth profiles of InGeO:F films before and after annealing obtained by SIMS are shown in **Fig. 4**. For the fluorinated film, F accumulates within the GeO_2 layer. After PDA, F becomes uniformly distributed throughout the GeO_2 and In_2O_3 layers and the overall F content decreases, which can be attributed to the desorption of volatile fluorides. This result highlights the buffer effect of GeO_2: without the GeO_2 layer, F would directly penetrate and accumulate in In_2O_3 during the initial fluorination stage, causing excessive ionic damage to the channel. The V_O consumption by GeO_2 is also observed in InGeO:F. As shown in **Fig. 5(a)**, with the etching position approaches the GeO_2/ In_2O_3 interface from the surface, the Ge *2p3/2* peak gradually shifts from Ge^{4+} to Ge^{2+}, indicating the GeO_2-to-GeO transformation. The deconvoluted Ge^{4+} and Ge^{2+} components ratio are plotted in **Fig. 5(b)**. **Fig. 6(a)** shows the In *3d* peak shifts from In–O to In–F, confirming F is bonded In. In **Fig. 6(b)**, the intensity of O *1s* remains nearly unchanged for the In_2O_3 and InGeO film, but the peak position shifts toward higher binding energy due the binding energy of O in Ge–O is higher than that in In–O [6],[7]. After fluorination, the intensity of O 1*s* decreases significantly, indicating that part of O is replaced by F. The fluorination mechanisms are illustrated in **Fig. 7**: F incorporation in In_2O_3 by both F/O substitution and F/V_O passivation, forming stable In–F bonds while reducing the excessive V_O defects, thereby improving channel conductivity and device stability. Meanwhile, during the fluorination process, the GeO_2 layer not only serves as a buffer to mitigate plasma-induced damage to the channel but also passivates V_O in In_2O_3.

4. Conclusion

In this study, the GeO_2 buffer layer was introduced into In_2O_3 films, followed by fluorination treatment. During fluorination, GeO_2 not only served as a buffer to effectively mitigate plasma-induced damage to the channel but also realized effective passivation of V_O during the subsequent annealing process. Meanwhile, F incorporation forms stable In–F bonds. This process not only increase the stability of overall *M-X* frame but also significantly suppressed the formation and migration of V_O . Consequently, the trap density was reduced, carrier scattering was weakened, and mobility was markedly enhanced, while the device exhibited improved stability under NBS.

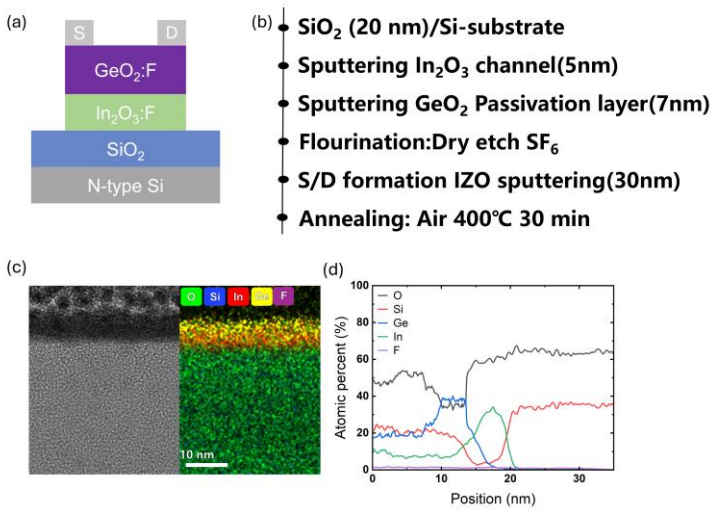

Fig. 1 Structure and characterization of the InGeO:F TFT (fluorine-doped indium oxide thin-film transistor). (a) Schematic of the device structure; (b) fabrication process; (c) cross-sectional TEM image with a channel thickness of 6 nm; (d) linear energy-dispersive X-ray spectroscopy (EDS) scan.

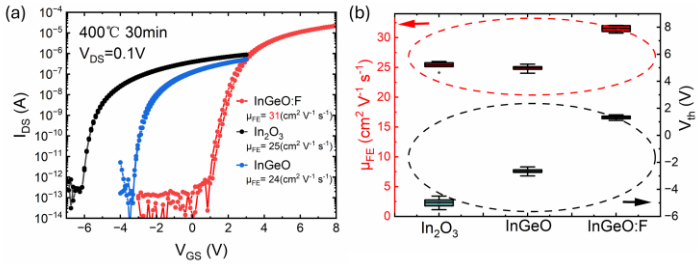

Fig. 2 (a) Transfer characteristics of In_2O_3 TFT, GeO_2-passivated In_2O_3 TFT, and GeO_2-passivated In_2O_3 TFT further treated with SF_6 dry etching; (b) extracted threshold voltage and mobility from the transfer characteristics.

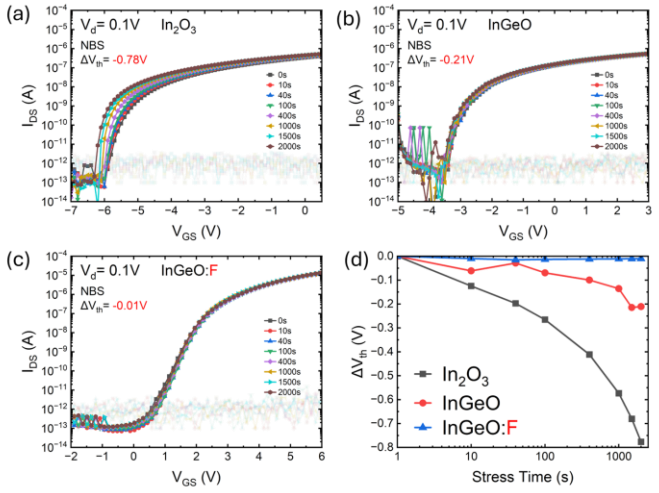

Fig. 3 Negative-bias stress (NBS) test results of three types of TFTs: (a) In_2O_3, (b) GeO_2-passivated In_2O_3, and (c) GeO_2-passivated In_2O_3 further treated with SF_6 dry etching; (d) evolution of threshold voltage shift (ΔV_{th}) with stress time for the three devices.

Acknowledgement: This research was funded by National Key Research and Development Program of China (Project No. 2022YFB3603902), National Natural Science Foundation of China (Grant No. 62304248), Outstanding Member Project of the Youth Innovation Promotion Association of the Chinese Academy of Sciences (CAS) No. Y2021046, and International Partnership Program (for Future Network) of the Chinese Academy of Sciences (Grant No.102GJHZ2022066FN).

Table Ⅰ Characteristic parameters of In_2O_3, InGeO, and InGeO:F TFTs, including μ_{FE}, V_{th}, SS, and ΔV_{th} under NBS conditions.

	V_{th} (V)	μ_{FE} ($cm^2 V^{-1} s^{-1}$)	SS (mV/dec)	NBS ΔV_{th} (V)
In_2O_3	-4.96	25	127	-0.78
InGeO	-2.67	24	97	-0.21
InGeO:F	1.25	31	90	-0.01

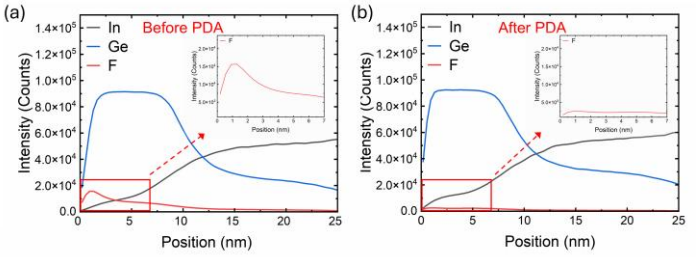

Fig. 4 SIMS elemental depth profiles of InGeO:F films before and after annealing.

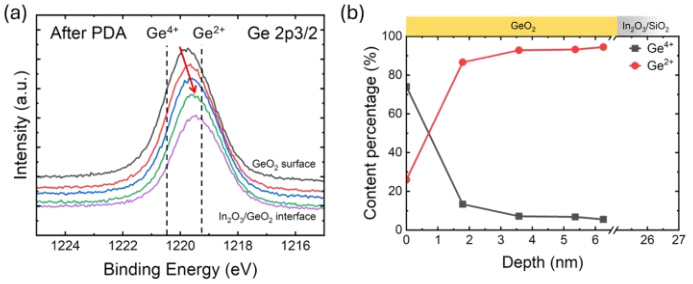

Fig. 5 (a) XPS depth profiling of the Ge-related peaks in the InGeO:F film; (b) variation of Ge^{4+} and Ge^{2+} valence state components as a function of depth.

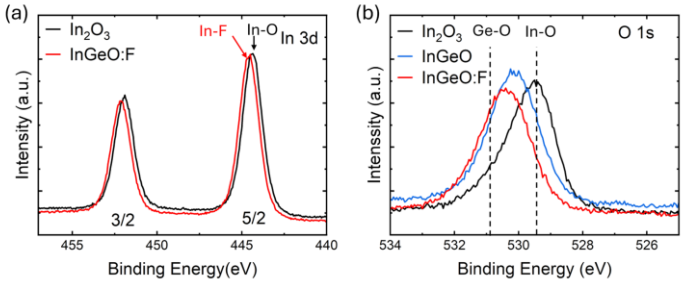

Fig. 6 XPS results: (a) In 3d spectra of In_2O_3 and InGeO:F films; (b) O 1s spectra of the three films.

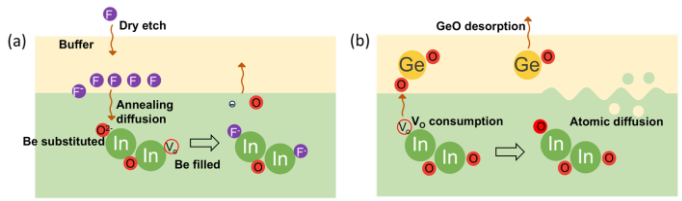

Fig. 7 Schematic illustration of the mechanism underlying the performance enhancement of InGeO:F devices. (a) F substitutes O, releases electrons and reduce scattering; (b) GeO_2 consumes oxygen vacancies to form GeO, which desorbs during annealing.

Reference:
[1] Ghaffarzadeh, K. *et al.*, Appl. Phys. Lett., 2010. **97**(11): p. 113504.
[2] Jung, K-M. *et al.*, International Display Workshops, 2019.
[3] Wang, Jiayi. *et al.*, VLSI Technology and Circuits, 2024.
[4] Rosendal, V. *et al.*, Physical Review B, 2024.
[5] Kim, Juwon. *et al.*, ACS Applied Electronic Materials. 2025.
[6] Gabás, M. *et al.* Applied surface science, 2012.
[7] Rajendran, V. *et al.* Engineering Reports, 2024.